Science of the Total Environment 749 (2020) 142086

Contents lists available at ScienceDirect

Science of the Total Environment

journal homepage: www.elsevier.com/locate/scitotenv

Enhancement of S(IV)-Cr(VI) reaction in p-nitrophenol degradation using rice husk biochar at neutral conditions

Kaikai Zhang [a], Peng Sun [a,b], Yu Zhang [a], Muthu Murugananthan [c], Kumaravel Ammasai [d], Yanrong Zhang [a,*]

[a] School of Environmental Science and Engineering, Huazhong University of Science and Technology, Wuhan 430074, PR China
[b] Institute of Energy and Environment, Inner Mongolia University of Science and Technology, Baotou 014010, PR China
[c] Department of Chemistry, PSG College of Technology, Coimbatore 641004, India
[d] Department of Chemistry, PSG Institute of Technology and Applied Research, Neelambur, Coimbatore, Tamilnadu, 641062, India

HIGHLIGHTS

- Sulfite could be activated by Cr(VI) to produce $SO_3^{\bullet-}$, $SO_4^{\bullet-}$ and •OH.
- The activation of sulfite by Cr(VI) was accelerated by biochar.
- Biochar could degrade organic pollutants by •OH production from O_2 activation.
- Both $SO_4^{\bullet-}$ and •OH contributed to the radical degradation of PNP.
- Cr(VI) was reduced by sulfite.

GRAPHICAL ABSTRACT

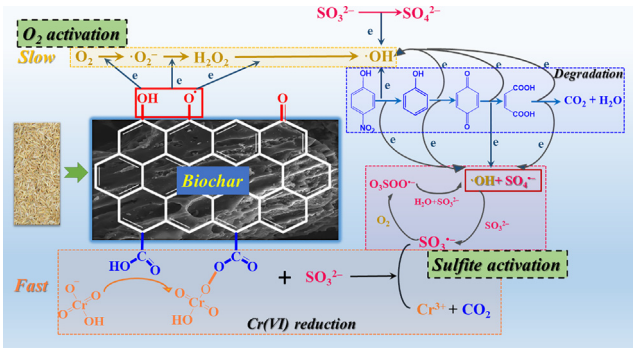

ARTICLE INFO

Article history:
Received 4 July 2020
Received in revised form 15 August 2020
Accepted 28 August 2020
Available online 31 August 2020

Editor: Baoliang Chen

Keywords:
Biochar
Cr(VI) reduction
Sulfite activation
O_2 activation
PNP degradation

ABSTRACT

In this study, biochar R550, obtained from rice husk charred at 550 °C, was used to detoxify Cr(VI) and organic pollutant p-nitrophenol (PNP) with the cooperation of sulfite, simultaneously. Cr(VI) was mainly reduced by sulfite, and the reduction was accelerated by biochar. Also, the reactive oxygen species formed in-situ as a result of enhanced oxidation of sulfite with Cr(VI)/R550 system and the activation of O_2 by R550, led to the degradation of PNP. Production of the radicals viz., $SO_3^{\bullet-}$, $SO_4^{\bullet-}$ and •OH was followed by Electron Paramagnetic Resonance (EPR) study, and the predominant role of $SO_4^{\bullet-}$ towards PNP degradation was confirmed by radical quenching tests. The reaction completed biochar sample was undergone the X-ray photoelectron spectroscopy (XPS) and Fourier Transform Infrared Spectroscopy (FTIR) spectral analysis, which suggested that the carboxyl group of the biochar triggered and enhanced the reactivity of Cr(VI) via coordination linkage, which in turn activated the sulfite and converted the SO_3^{2-} into $SO_4^{\bullet-}$ to a higher extent by overcoming the undesirable transformation of SO_3^{2-} to SO_4^{2-}. Such results could also be verified by the other three biochar (Oxi-R550, H-R550, and R800). The results of the present study shed light on the mechanism of biochar mediated sulfite activation process by Cr(VI) and also assured the viability and green approach of the technique in detoxifying the industrial effluents containing Cr(VI) and organic pollutants.

1. Introduction

Chromium is one of the important heavy metals that let out in the effluent stream of electroplating, mining, leather tanning, and textile industries. The existence of chromium in the wastewater at neutral pH

* Corresponding author.
E-mail address: yanrong_zhang@hust.edu.cn (Y. Zhang).

https://doi.org/10.1016/j.scitotenv.2020.142086
0048-9697/

is mostly in hexavalent state Cr(VI) (Gil-Cardeza et al., 2014), and the usual coexisting organic pollutants are phenol, trichloroethylene, atrazine, etc. (Mytych and Stasicka, 2004; Wang et al., 2013; Wang et al., 2019; Zhang et al., 2016). For instance, in discharged effluent from the tannery industries, 0.1–20 mg/ L of Cr(VI) and 0–50 mg/L of phenolic compounds such as phenol, PNP, and p-cresol could be detected (Cao et al., 2016; Davoudi et al., 2014; Shakir et al., 2012; Zewdu et al., 2018). The existing treatment techniques have mainly addressed the removal of Cr(VI) with priority (Habibul et al., 2016; Jiang et al., 2014; Liu et al., 2016), and not the fate of recalcitrant and acutely toxic organic pollutants that coexist. Further, though the adsorption and advanced oxidation process techniques were widely adopted to treat the organic pollutant contaminated wastewaters (Hu et al., 2019; Liu et al., 2019; Lu and Chen, 2018; Teixido et al., 2013), they severely suffer from a poor performance owing to coexisting Cr(VI). For instance, the adsorption efficiency of biochar towards organic pollutants removal was influenced by Cr(VI) (Zhang et al., 2019a; Zhang et al., 2015). Also, Cr(VI), a typical electron quencher, retards the rate of degradation of the organic pollutants, when the system contains O_2, H_2O_2, and persulfate (Fang et al., 2014; Zhang et al., 2019a). Hence, it is important to develop an effective method for decontaminating wastewater that contains both Cr (VI) and organic pollutants.

$$SO_3^{2-} + h\nu \leftrightarrow SO_3^{\cdot -} + e_{aq}^{-} \quad (1)$$

The sulfite-based method has been successfully used to treat Cr(VI) and organic pollutants recently (Jiang et al., 2018; Jiang et al., 2015; Yuan et al., 2016). In this method, sulfite was reported to favor both the reduction and oxidation of the organic pollutants. The reduction step proceeds via hydrated electron (e_{aq}^{-}), which is generated with UV rays in the absence of O_2 (Reaction 1) (Gu et al., 2016; Li et al., 2012), and the oxidation is possible by reactive oxygen species (ROS), formed in the presence of O_2 (Du et al., 2017; Liu et al., 2017; Xu et al., 2016a; Zhang et al., 2017). Furthermore, the reaction between sulfite and Cr (VI) could generate ROS, which facilitates the degradation of coexisting organic pollutants. Herein, the Cr(VI) could react with two sulfite ions (Reactions 2 and 3) to form a complex $[CrO_2(SO_3)_2]^{2-}$, which spontaneously undergoes a disproportionation reaction and generates $SO_3^{\bullet -}$ radical (Reaction 4) (Jiang et al., 2015; Jiang et al., 2016; Yuan et al., 2016). The $SO_3^{\bullet -}$ generated, is transformed into $SO_5^{\bullet -}$, $SO_4^{\bullet -}$ and •OH by the influence of O_2 presented (Reactions 5, 6, and 7).

$$HCrO_4^{-} + HSO_3^{-} \leftrightarrow CrSO_6^{2-} + H_2O \quad (2)$$

$$CrSO_6^{2-} + SO_2 \leftrightarrow CrO_2(SO_3)_2^{2-} \text{ (rate determining step)} \quad (3)$$

$$CrO_2(SO_3)_2^{2-} + 4H_2O + 2H^+ \leftrightarrow SO_4Cr(H_2O)_5^{+} + SO_3^{\cdot -} \quad (4)$$

$$SO_3^{\cdot -} + O_2 \rightarrow O_3SOO^{\cdot -} \; k = 2.5 \times 10^9 \; M^{-1} \; s^{-1} \quad (5)$$

$$SO_3^{2-} + O_3SOO^{\cdot -} \rightarrow SO_4^{\cdot -} + SO_4^{2-} \; k = 1.3 \times 10^7 \; M^{-1} \; s^{-1} \quad (6)$$

$$SO_4^{\cdot -} + H_2O \rightarrow SO_4^{2-} + {}^{\cdot}OH + H^+ \; k = \left(10^3\text{–}10^4\right) \; M^{-1} \; s^{-1} \quad (7)$$

$$SO_4^{\cdot -} + HSO_3^{-} \rightarrow HSO_4^{-} + SO_3^{\cdot -} \; k = (2.6\text{–}8) \times 10^8 \; M^{-1} \; s^{-1} \quad (8)$$

$${}^{\cdot}OH + HSO_3^{-} \rightarrow H_2O + SO_3^{\cdot -} \; k = 4.6 \times 10^9 \; M^{-1} \; s^{-1} \quad (9)$$

$$CrSO_6^{2-} + H^+ + HCrO_4^{-} \leftrightarrow O_3CrOCrO_2SO_3^{2-} + H_2O \quad (10)$$

$$O_3CrOCrO_3SO_3^{2-} \rightarrow 2Cr(V) + SO_4^{2-} \quad (11)$$

$$Cr(VI) + SO_3^{\cdot -} \leftrightarrow Cr(V) + SO_4^{2-} \quad (12)$$

$$Cr(V) + SO_3^{\cdot -} \rightarrow Cr(III) + SO_4^{2-} \quad (13)$$

However, the S(IV)-Cr(VI) system suffers from the following limitations in degrading the organic pollutants. Firstly, the sulfite ion, comparing to the usual organic contaminants, gets reacted with $SO_4^{\bullet -}$ and •OH with priority (Reaction 8, $k = (2.6\text{–}8) \times 10^8 \; M^{-1} \; s^{-1}$; Reaction 9, $k = 4.6 \times 10^9 \; M^{-1} \; s^{-1}$) (Xie et al., 2019; Zhang et al., 2018a; Zhang et al., 2017). Secondly, the complex $O_3CrOCrO_3SO_3^{2-}$ formed as a by-product of the reaction between sulfite and Cr(VI), is unable to generate ROS (Reactions 10 and 11). Also, the $SO_3^{\bullet -}$ can be consumed by Cr(VI) and Cr(V) at the cost of $SO_5^{\bullet -}$, $SO_4^{\bullet -}$ and •OH generations. Another limitation is the redox potential of Cr(VI) gets affected, as the pH of the reaction system raises, which reflects a decline in the reaction between Cr (VI) and sulfite (Jiang et al., 2015; Yuan et al., 2016). Owing to these limitations, the refractory organic pollutants such as p-nitroaniline, 2,6-dinitrophenol, and bisphenol-A get hardly degraded in the S(IV)-Cr(VI) system at neutral pH conditions (Yuan et al., 2016). Thus, increasing the efficiency of sulfite at neutral pH conditions could help detoxify the complex wastewater containing Cr(VI) and organic pollutants.

The biochar, an attractive remediation additive, has exhibited an excellent performance on the reduction of Cr(VI) and degradation of organic pollutants. For instance, the removal of Cr(VI) could be facilitated by the redox-active functional groups of biochar material viz. carboxyl and phenolic hydroxyl as well as the persistent free radicals via reduction, complexation, and co-precipitation methods (Chen et al., 2015; Diao et al., 2018; Dong et al., 2014; Xu et al., 2019). And, the process of organic pollutant degradation caused the radicals generated through O_2, H_2O_2, and $S_2O_8^{2}$ activation (Fang et al., 2014; Fang et al., 2015a; Zhang et al., 2018b), could further be promoted by phenolic hydroxyl as well as persistent free radicals. Besides, biochar could also mediate the electrons transfer between two redox components. For instance, the reduction of hematite, trichloroethylene, and 2,4-dinitrotoluene by dissimilatory metal-reducing bacteria Shewanella oneidensis MR-1, sulfides, and zerovalent iron, respectively, could be facilitated by biochar (Ding et al., 2018; Oh et al., 2012; Oh et al., 2002; Xu et al., 2016b). Therefore, it was proposed that biochar could facilitate the reduction of Cr(VI), especially when other reductants exist.

In this study, the primary objective was to examine the possibility of biochar material cooperating with sulfite in detoxifying the complex system of Cr(VI) and organic pollutants at neutral pH conditions. PNP was selected as a model organic pollutant, because of its toxic characteristic nature and prominence in the effluents of pharmaceutical, petrochemical, and pesticide industries. The accelerated reaction between Cr(VI) and sulfite and the enhanced degradation of PNP with biochar material were investigated. The results obtained here could provide new insight into the biochar mediated sulfite activation process by Cr (VI), which is of significant interest in detoxifying the industrial effluents containing multiple pollutants such as Cr(VI) and organics.

2. Materials and methods

2.1. Materials and chemicals

The details of the chemicals used in this study are given in the Supporting information (SI; Text S1). The methods adopted for the preparation and characterization of the biochar material are given in Table S2, Fig. S1, Text S2, and Text S3, which have already been explored in earlier studies (Zhang et al., 2019a; Zhang et al., 2018b).

2.2. Experimental process

The experiments were carried out using a 200 mL glass beaker at 25 ± 2 °C in the usual lighting conditions in our laboratory. A defined quantity of PNP (0.04 mM) and Na_2SO_3 (0–10 mM) was added in the reaction solution and its pH was adjusted to 7, using 0.1 M of NaOH and H_2SO_4. This was because the effluents containing Cr(VI) discharged from the industries possessed a neutral pH, such as tannery (Szpyrkowicz et al., 2005), iron and steel (Das et al., 2018). Then, a desired

quantity of Cr(VI) (0–0.4 mM) and the biochar material (0.2, 0.5 and 1 g L^{-1}), were added into the solution under constant stirring. At fixed reaction time intervals, a defined volume of sample was siphoned out. In 1 mL of the sample, a mixture of 0.9 mL of methanol and 0.1 mL of NaOH was added to arrest the reactivity of the radicals on PNP degradation and desorb the remaining unreacted PNP from the biochar surface. Then the sample was filtered using a 0.22 μm Poly Tetra Fluoro Ethylene (PTFE) membrane, and its PNP concentration was determined with a UV–vis spectrophotometer fixing the absorbance at 400 nm. Another 1 mL of the siphoned out sample was filtered through a 0.22 μm PTFE membrane for determining its Cr(VI) concentration by colorimetric method using a complex regent 1,5-diphenylcarbazide and total Cr concentration using Inductively Coupled Plasma Optical Emission Spectrometer (ICP-OES) (Habibul et al., 2016). Quenching studies were conducted to investigate the influence of ROS on PNP degradation. 40 mM of tert-butanol (TBA) was used for quenching the •OH because the reaction constant between TBA and •OH is 3.8–7.6 × 10^8 L M^{-1} s^{-1}, which is about 1000 times higher than the reaction constant observed between TBA and SO_4•$^-$ (4.4–9.1 × 10^5 L M^{-1} s^{-1}) (Duan et al., 2018; Kang et al., 2018). 4 mM of aniline was used to quench both SO_4•$^-$ and •OH. This was because the rate constants of the reaction of aniline with SO_4•$^-$ as well as •OH, are in the order of 10^9 L mol^{-1} s^{-1}, which is nearly three orders of a larger magnitude than that observed for aniline with SO_5•$^-$ (k = 3.0 × 10^6 L M^{-1} s^{-1}) and SO_3•$^-$ (k < 1.0 × 10^6 L M^{-1} s^{-1}). The reproducibility of the analytical tests was checked in triplicate.

2.3. Analytical method

The concentration of PNP was determined with a UV–vis spectrophotometer (Evolution 201, Thermo Scientific, USA) fixing absorbance at 400 nm and the pH of the aqueous solutions was monitored by Sartorius PB-10 pH meter equipped with Sartorius pH/ATC electrode. The concentration of sulfite presented in the solution was determined by adopting a modified colorimetric procedure of DTNB [5,5′-dithiobis-(2-nitrobenzoic acid)] (Dong et al., 2020). In brief, 1 mL of the sample was transferred into a cuvette wherein a mixture of 1 mL of EDTA (Ethylene Diamine Tetraacetic Acid, 1 mM), 2 mL of DTNB (1 mM), and 5 mL of Na_2HPO_4/KH_2PO_4 buffer (pH 7) was taken. Upon the color development until 15 min, the absorbance of the sample solutions at 412 nm was detected with a UV–vis spectrophotometer. The remaining concentration of Cr(VI) in the solution was determined by adopting the diphenylcarbazide method (Zhang et al., 2019b). A mixture of concentrated acids viz. H_3PO_4, H_2SO_4, H_2O with a volume ratio of 1:1:2, respectively, was taken and mixed with diphenylcarbazide reagent to minimize interference of acids in the determination of Cr(VI). Upon an intense color development (>15 min), the absorbance of the sample solutions was detected at 540 nm. The total concentration of Cr in the supernatant was analyzed by Inductively Coupled Plasma Optical Emission Spectroscopy (ICP-OES, Optima 8300+, PerkinElmer, America) after preserving samples with 2% (v/v) ultrahigh-purity nitric acid. The intermediates formed during the degradation of PNP were monitored and their concentrations were determined by Liquid Chromatography coupled with a mass analyzer system (LC-MS, 1100 LC/MSD Trap, Agilent, USA). The occurrence of radical species such as $SO_4^{\cdot-}$ and ·OH was examined with an electron paramagnetic resonance (EPR) spectroscopy (ELEXYS E580, Bruker Co.) using 100 mM 5,5-dimethyl-1-pyrroline N-oxide (DMPO) as a spin-trapping agent. The detailed operating parameters for ICP-OES, LC-MS, EPR were provided in Text S2 and Table S1.

3. Results and discussion

3.1. Activation of sulfite by Cr(VI) in biochar system

Fig. 1a displayed the changing trend of PNP concentration after the extraction, and the extraction was conducted using the methanol solution containing NaOH to desorb the residual PNP on biochar. Thus, the decrease of PNP concentration in Fig. 1a was mainly owing to the degradation rather than the adsorption. As for the biochar system, the removal efficiency of PNP was observed to be only 36.6% under the conditions that the initial concentration of PNP, the dosage of R550, and the solution pH were 0.04 mM, 1 g L^{-1} and 7, respectively. The degradation reaction was followed by the first-order kinetics model with a greater R-square (R^2 = 0.9872) (Fig. S2), and accordingly, the rate constant was calculated to be 0.0017 min^{-1}. The activation of O_2 by the reductive groups of R550 leads to form •OH progressively, which degrades the PNP molecule. According to our earlier studies (Zhang et al., 2019a; Zhang et al., 2018b; Zhong et al., 2019), phenolic hydroxyl groups with the hydroquinone-like structure and semiquinone-type radicals on biochar possessed the reducibility, which could donate electrons to O_2 to facilitate the production of •OH via sequential transformations of O_2 to O_2•$^-$, O_2•$^-$ to H_2O_2 and H_2O_2 to •OH. However, upon addition of sulfite (5 mM) in the system, the degree of PNP degradation declined from 36.6 to 26.6% in 360 min (Fig. 1a), owing to the higher reducing power of sulfite and its fast reaction rate constant with •OH (k = 4.6 × 10^9 M^{-1} s^{-1}). Thus, sulfite got oxidized with priority by •OH at the cost of degradation of the recalcitrant PNP molecule. The increased rate of sulfite oxidization observed from 47.2 to 71.8% at 360 min, is evidence for this (Fig. 1c).

On the other hand, the addition of Cr(VI) activates the sulfite ions which could facilitate the degradation of the PNP molecule. While adding 0.2 mM concentration of Cr(VI) into a sulfite system (5 mM), the reaction period taken for attaining 36.1% degradation was reduced from 360 min into a shorter period of 90 min (Fig. 1a), with complete utilization of sulfite ions (Fig. 1c), however, the sulfite alone has no impact on the degradation of PNP (Fig. 1a). Furthermore, the addition of R550 into the system, enhances the degradation of PNP, as a result of the acceleration of the reaction between Cr(VI) and sulfite. As shown in Fig. 1a, the degradation of PNP to an extent of 51.5% could be attained within a reaction period of 30 min with a rate constant value of 0.0272 min^{-1}. The observed rate constant with Cr(VI)/R550 system was greater than that for the S(IV)-Cr(VI) system of 90 min and R550 system of 360 min (Fig. S2). In the meantime of 30 min reaction period, the removal efficiencies of Cr(VI) and sulfite ions were promoted to 92.8% (Fig. 1b) and 93.7% (Fig. 1c), respectively. It suggests that the reaction of Cr(VI) towards sulfite, was accelerated on R550, which leads to enhanced degradation of PNP. Moreover, the pH of the S(IV)-Cr(VI) system decreased from 7 to 4.6, mainly owing to the oxidization of sulfite. Such decreasing pH boosted the Cr(VI) reduction by sulfite, production of ROS from sulfite activation, and PNP degradation.

To exclude the adsorption of Cr(VI), the removal efficiency of total chromium [Cr(VI) + Cr(III)] measured and was only 31.5% in the R550-S(IV)-Cr(VI) system, which was less than the 92.8% of removal efficiency for Cr(VI). It suggested that most of Cr(VI) was mainly reduced to Cr(III) in the solution. Besides, the adsorption chromium on biochar could be confirmed by XPS. As shown in Fig. S3, the two characteristic peaks of Cr $2p_{1/2}$ at 587.8 eV and $2p_{3/2}$ at 578.2 eV, were measured on R550 after the reaction, demonstrating the adsorption of chromium during the reaction. According to previous studies, biochar possessed weak capacity on the Cr(VI) removal under neutral condition, and 1 g L^{-1} of R550 only possessed 4% of removal efficiency towards 0.2 mM Cr(VI) under neutral condition, while the removal efficiency of Cr(VI) by biochar increased to 28.5% at pH 4 (Zhang et al., 2019b). Thus, most of Cr(VI) in the R550-S(IV)-Cr(VI) system was mainly reduced by sulfite. Besides, as shown in Fig. S2b, the R550, improved the utilization efficiency of sulfite ion towards PNP degradation, and the utilization rate constant with S(IV)-Cr(VI) system increased by threefold from 0.0308 min^{-1} to 0.0951 min^{-1} upon adding R550. In the degradation front, the rate of degradation of PNP was seven times higher with the R550 added S(IV)-Cr(VI)-system.

Even upon completion of sulfite and Cr(VI) transformations, in the initial 60 min of R550 presented system, the degradation of PNP was

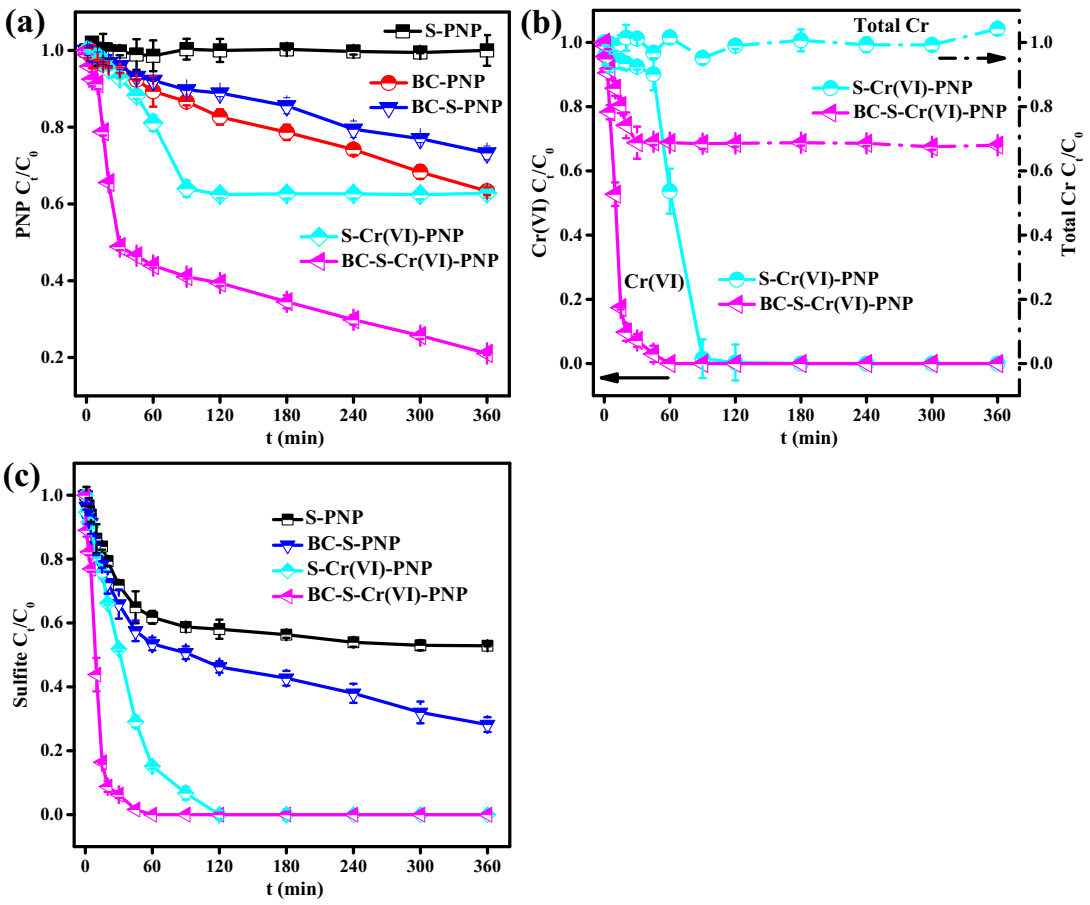

Fig. 1. Performance of (a) PNP degradation, (b) Cr(VI) reduction, and (c) sulfite decomposition in sulfite, R550, R550/sulfite, sulfite/Cr(VI) and R550/sulfite/Cr(VI) systems. Reaction conditions: $[PNP]_0 = 0.04$ mM, $[Cr(VI)]_0 = 0.2$ mM, $[sulfite]_0 = 5$ mM, $[Biochar]_0 = 1$ g L^{-1}, pHini = 7.

proceeding up to 360 min showing 79% removal (Fig. 1a), with almost a similar reaction rate (0.0021 min^{-1}) compared to that (0.0017 min^{-1}) of sole R550 system. It indicates that the pre-reaction between Cr(VI) and sulfite did not influence the further carryover of the reaction by R550 that activates O_2, by which the degradation of PNP continues. It also suggests that the redox moiety of the R550 was responsible for the activation of O_2, which is not influenced or connected with the S(IV)-Cr(VI) reaction system.

3.2. Identification of reactive oxidants

Figs. 2a, b, and S4 exhibited the decline of PNP degradation as the quenchers TBA and aniline were added. Upon introducing TBA, a slight decrease of PNP degradation from 37.2 to 34.5%, was observed with S(IV)-Cr(VI) system (Figs. 2a and S4a), in contrast to a notable decrease of 79 to 56.3% against the R550-S(IV)-Cr(VI) system (Figs. 2b and S4b). It suggests that the contribution of •OH towards PNP degradation was considered one with the latter system unlike the former. The result was confirmed by analyzing the radicals with EPR. As shown in Figs. 2c and S5, the presence of DMPO−•OH adduct was found in neither S(IV)-Cr(VI) nor R550 systems, but a remarkable concentration was detected in the R550-S(IV)-Cr(VI) system. There are two possible ways of forming the •OH: the activation of sulfite by Cr(VI) could have been accelerated which results in the generation of ROS; or else, the biochar mediated O_2 activation reaction could be enhanced in the presence of sulfite and Cr(VI). However, the latter was proved to be practically impossible. Because it was observed in one of our earlier studies (Zhang et al., 2019a), that the generation of •OH is suppressed by Cr(VI) in the R550 system. Additionally, as seen in Fig. 1c, the consumption of •OH by sulfite ion owing to its high reducing power could be another factor.

Since the concentration of aniline introduced, was 100 times higher than that of PNP, the degradation of PNP was completely arrested in the S(IV)-Cr(VI) system, and it was only 10% in the R550-S(IV)-Cr(VI) system (Fig. 2a and b). The degradation of PNP was mostly because of $SO_4^{\bullet-}$ in the S(IV)-Cr(VI) system not by the R550. Moreover, the generation of $SO_4^{\bullet-}$ and •OH was facilitated by R550 through the activation of sulfite by Cr(VI). As shown in Fig. 2c, in the simple S(IV)-Cr(VI) system, the adduct of DMPO−$SO_3^{\bullet-}$ was generated initially and the adduct of DMPO−$SO_4^{\bullet-}$ was found later at 20 min. However, with the R550 added S(IV)-Cr(VI) system, a larger quantity of $SO_4^{\bullet-}$ and •OH was generated in the initial phase of 3 min (Fig. 2d).

3.3. Role of biochar in enhancing S(IV)-Cr(VI) reaction

The C 1s XPS spectra of R550 can be deconvoluted into four peaks of 285.0, 286.4, 287.8, and 289.6 eV, which correspond to C-C/C=C, C—O, C=O, and COO^- groups, respectively, as shown in Fig. 3a. After completion of the degradation reaction in the simple R550 system, the relative intensity observed against the functional groups of C=O and COO^- was increased as shown in Fig. 3b. As described in Table 1, the relative percentage was increased from 3.03 to 4.27% for C=O and from 5.38 to 6.73% for COO^-, whereas for the reductive functional groups viz. C-C/C=C and C—O, it was decreased from 74.83 to 73.96%, and from 16.75 to 15.03%, respectively. As reported in the earlier studies (Fang et al., 2017; Fang et al., 2015b), the activation of O_2 occurs via the oxidization of biochar that results in the formation of •OH which causes the radical degradation of organic pollutants.

After the degradation process, the carbon composition of R550 varied remarkably (Fig. 3c) in the R550-S(IV)-Cr(VI) system compared with those of the solo R550 (Fig. 3a) and R550-PNP systems (Fig. 3b).

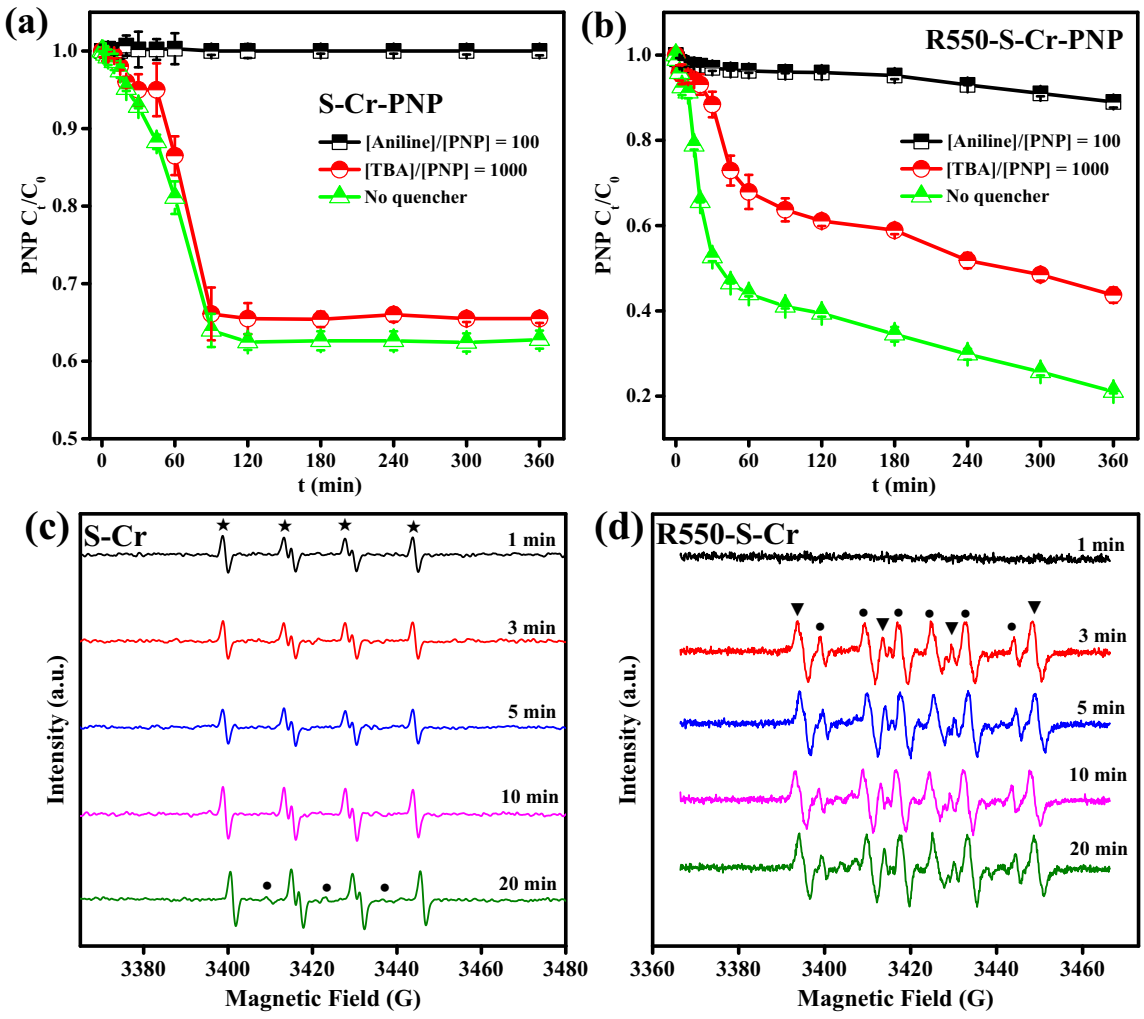

Fig. 2. Profile of PNP degradation with time in (a) S(IV)-Cr(VI) and (b) R550-S(IV)-Cr(VI) system with radical scavengers. Reaction conditions: $[PNP]_0 = 0.04$ mM, $[Aniline]_0/[PNP]_0 = 100$, $[TBA]_0/[PNP]_0 = 1000$, $[Cr(VI)]_0 = 0.2$ mM, $[sulfite]_0 = 5$ mM, $[Biochar]_0 = 1$ g L^{-1}, pHini = 7. EPR spectrum of free radicals from (c) S(IV)-Cr(VI) and (d) R550-S(IV)-Cr(VI) systems. ★ refers to DMPO−SO_3•$^-$ adduct, ● to DMPO−SO_4•$^-$ adduct and ▼ to DMPO −•OH adduct. Reaction conditions: $[DMPO]_0 = 100$ mM, $[Cr(VI)]_0 = 0.2$ mM, $[sulfite]_0 = 5$ mM, $[Biochar]_0 = 1$ g L^{-1}, pHini = 7.

As shown in Table 1, the relative percentage of C—O and C═O groups of the simple R550 was decreased and increased, respectively. The extent of variation of C—O and C═O was comparable in both R550-PNP and R550-S-Cr-PNP systems. It suggests that the activation of O_2, rather than the reaction between sulfite and Cr(VI), reflects as a decrease of C—O and an increase of C═O with the R550 of both the systems. However, unlike the R550-PNP system, a decrease of COO^- (from 5.38 to 4.83%) and an increase of C-C/C=C (from 74.83 to 75.52%) of R550 was observed in the R550-S(IV)-Cr(VI)-PNP system, indicating that COO^- and C-C/C=C are involved in the reaction of the S(IV)-Cr(VI). As reported in the earlier studies (Jiang et al., 2018; Jiang et al., 2016), the COO^- of polycarboxylate could coordinate with Cr(VI) that forms polycarboxylate-$CrSO_6^{2-}$, as per the reaction-14. Thus, similar coordination between Cr(VI) with COO^- could also be expected on the biochar, which causes the acceleration of reduction of Cr(VI) via sulfite, and forms SO_3•$^-$ by a quick decomposition according to the reaction-15 (Jiang et al., 2018; Jiang et al., 2016).

$$CrSO_6^{2-} + \text{polycarboxylate} \leftrightarrow \text{polycarboxylate}-CrSO_6^{2-} \quad (14)$$

$$\text{polycarboxylates}-CrSO_6^{2-} \leftrightarrow \text{polycarboxylate}-Cr(V) + SO_3^{\cdot -} \quad (15)$$

Additionally, the variation of C content on biochar after completion of the reaction was analyzed. The amount of Si was chosen as a standard value for normalization to reduce the deviation of XPS measurements among the different batches, due to its inert reactivity during the reaction (Xiao et al., 2014). As shown in Table 1, the ratio of superficial C/Si decreased from 19.31 to 17.72 after completion of the degradation reaction in the R550-S(IV)-Cr(VI) system, while no change in the solo R550 reaction system. It means that the C species were partially removed from the biochar due to the sulfite activation reaction by Cr(VI). In the R550-S(IV)-Cr(VI) system, the decrease of COO^- and C—O was observed upon the degradation of PNP, in which, the decline of C—O could probably be originated from the oxidization of R550 by O_2 which is caused for the slight variation of C/Si (Fig. 3b, R550-PNP system). Thus, the decrease of C/Si should have been originated from the removal of COO^-. Furthermore, the removal of COO^- reflects as the enlarged relative proportions of C-C/C=C, C—O, and C═O in the C compositions of biochar surface, which was confirmed by the increase of C-C/C=C, C—O and C═O of R550 in the R550-S(IV)-Cr(VI) system (Table 1).

The complex between COO^- on biochar and Cr(VI) could lead to the reduction of Cr(VI) on biochar, and the structural change and the decline of COO^- on biochar. Fig. 3d displayed the transformation of the functional groups on the biochar material using FTIR upon the PNP degradation and S(IV)-Cr(VI) reaction. In the R550-S(IV)-Cr(VI) system, the peak corresponding to C═O of COO^- (carboxyl) was shifted from 1693 to 1698 cm^{-1} due to its persistency after forming a complex with Cr(VI)

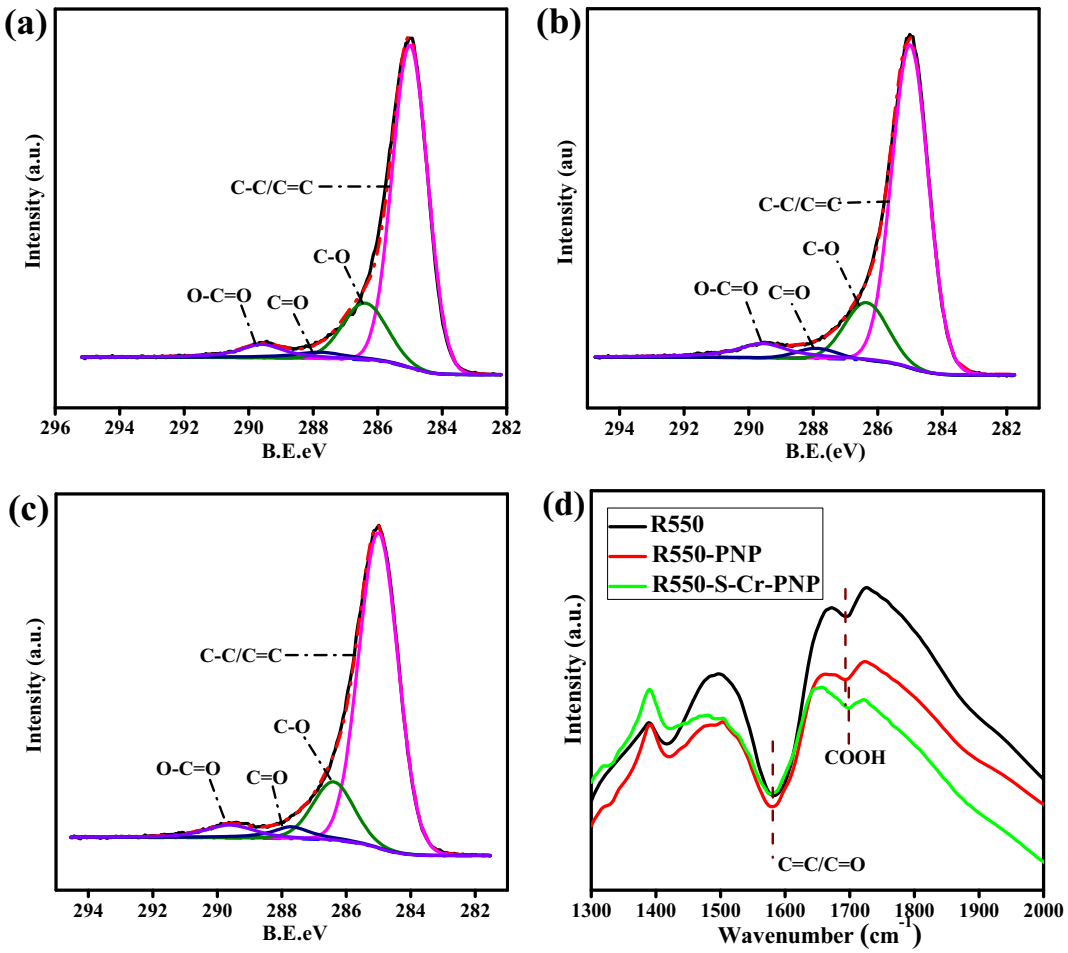

Fig. 3. C 1s XPS spectra of R550 (a) before and after PNP degradation in the (b) absence and (c) presence of S(IV)-Cr(VI) reaction. (d) Comparison of FTIR spectra of original R550 and after PNP degradation in the absence and presence of S(IV)-Cr(VI) reaction. Reaction conditions: $[PNP]_0 = 0.04$ mM, $[Cr(VI)]_0 = 0.2$ mM, $[sulfite]_0 = 5$ mM, $[Biochar]_0 = 1$ g L^{-1}, pHini = 7.

by electron donation (Dong et al., 2014). The shift was neither due to the activation of O_2 nor the degradation of PNP by R550, as the COO^- of biochar is not involved in the processes. Besides, the two characteristic peaks Cr $2p_{1/2}$ at 587.8 eV and $2p_{3/2}$ at 578.2 eV, detected for R550 (Fig. S3) after the reaction, which were lower than 588.7 eV of Cr(VI) $2p_{1/2}$ and 578.5 eV of Cr(VI) $2p_{3/2}$, respectively. It indicated that Cr(VI) accepted electrons from the functional groups on R550. Thus, the comprehensive analysis of FTIR and XPS demonstrated the complex between Cr(VI) and COO^- on biochar. Such a conclusion differed from the removal mechanism of Cr(VI) by biochar at acidic conditions. As reported in the earlier study, biochar derived from rice husk (R550) demonstrated an excellent performance towards Cr(VI) removal via the reduction, and the maximum adsorption capacity of 4.33 mg g^{-1} could be attained for R550 at pH 3 (Zhang et al., 2019b). By analyzing the transformation of reactive moieties on biochar upon the Cr(VI) removal, phenolic hydroxyl groups with the hydroquinone-like structures and semiquinone-type radicals on biochar involved in the Cr(VI) reduction under acidic pH 2– 4 via donating electrons (Dong et al., 2014; Xu et al., 2019; Zhong et al., 2018). As a contrast, as the pH of the reaction system raised to 7, the poor efficiency of Cr(VI) removal by biochar was achieved, owing to the decreasing oxidizing ability of Cr(VI) under neutral conditions. However, the existence of COO^- on polycarboxylates, humic acid, and small molecular weight organic acids could enhance the Cr(VI) reduction by sulfite, magnetite, and zero-valent iron under neutral conditions, respectively (Jiang et al., 2018; Jiang et al., 2014; Rivero-Huguet and Marshall, 2009). Such an enhancement could be ascribed to the complex between Cr(VI) and COO^- on organic compounds (Jiang et al., 2012), which could enlarge the activity of Cr(VI), thus resulting in the promoted Cr(VI) reduction. A similar conclusion could also be obtained in this study. The COO^- on biochar enhanced the reduction of sulfite by Cr(VI) via forming the complex with Cr(VI) under neutral conditions.

Hence, as illustrated in Scheme 1, it was inferred that the COO^- of R550 could probably form complexes with $CrSO_6^{2-}$ (Reaction 16) to enhance the reactivity of Cr(VI), thereby the activation of sulfite ions and in turn the formation of $SO_3^{\bullet-}$ via intramolecular electron transfer reaction (Reaction 17). Herein, the COO^- serving as an electron donor could facilitate the reduction of Cr(VI) as well (Reaction 18). Also, the formation of the complex BC-COO^--$CrSO_6^{2-}$ prevented the reaction of $CrSO_6^{2-}$ with another $HCrO_4^-$ and in turn the production of $O_3CrOCrO_3SO_3^{2-}$ (Reactions 10 and 11). Besides, as shown in Scheme 1, phenolic hydroxyl groups with hydroquinone-like structures and semiquinone-type radicals on biochar could activate O_2 slowly, thus resulting in the sluggish OH production and slight PNP degradation by the solo biochar.

$$CrSO_6^{2-} + BC{-}COO^- \leftrightarrow BC{-}COO^-{-}CrSO_6^{2-} \quad (16)$$

Table 1
C composition for R550 based on XPS Analysis after PNP degradation in the absence and presence of S(IV)-Cr(VI) reaction. Reaction conditions: $[PNP]_0 = 0.04$ mM, $[Cr(VI)]_0 = 0.2$ mM, $[sulfite]_0 = 5$ mM, $[Biochar]_0 = 1$ g L^{-1}, pHini = 7.

	C/Si	O/Si	C-C/C=C	C-O	C=O	COO^-
R550	19.31	2.98	74.83%	16.75%	3.03%	5.38%
R550-PNP	19.46	3.06	73.96%	15.03%	4.27%	6.73%
R550-S-Cr-PNP	17.72	3.01	75.32%	15.39%	4.46%	4.83%

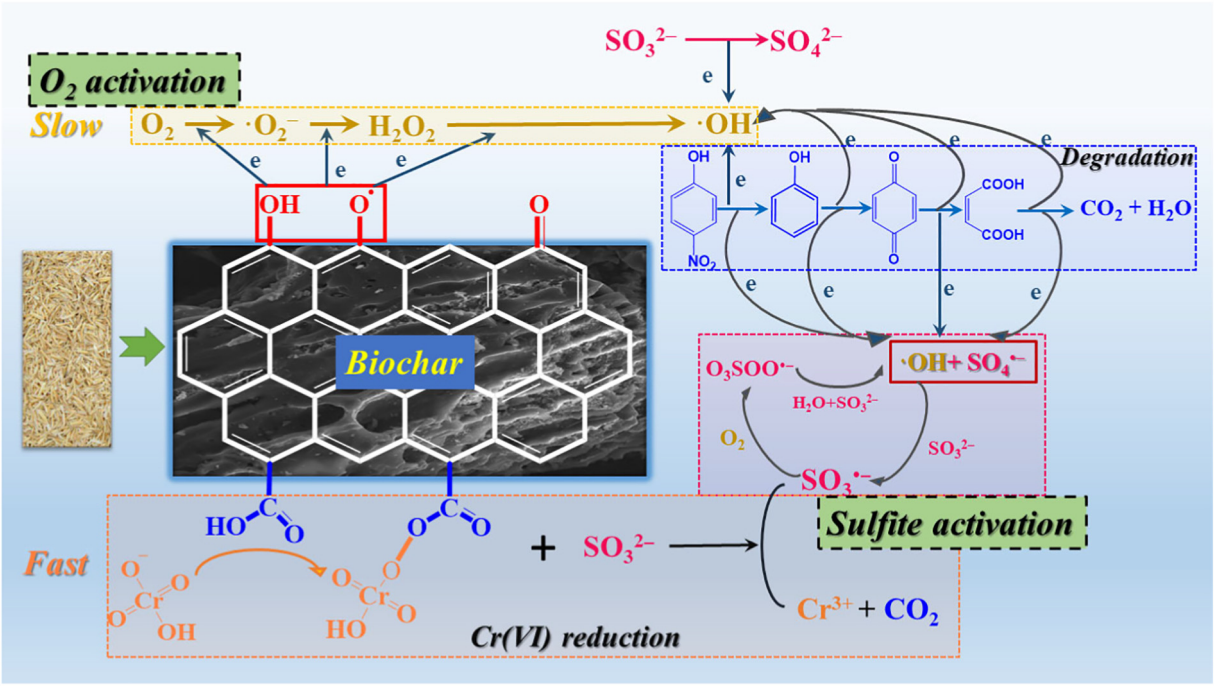

Scheme 1. ROS generation and PNP degradation from the biochar coexisting S(IV)-Cr(VI) system

$$BC{-}COO^{-}{-}CrSO_6^{2-} \leftrightarrow BC{-}COO^{-}{-}Cr(V) + SO_3^{\cdot -} \quad (17)$$

$$BC{-}COO^{-}{-}Cr(V) \leftrightarrow BC + CO_2 + Cr(III) \quad (18)$$

3.4. Impact of COO^- on the reaction of activation of sulfite by Cr(VI)

For biochar R550, the changes of C composition before/after reactions detected by the XPS were subtle. To further validate the effect of COO^- on the activation of sulfite by Cr(VI), two different types of biochar viz. Oxi-R550 and H-R550 were prepared by treating with H_2O_2 and $NaBH_4$, respectively, which were utilized in the S(IV)-Cr(VI) reaction. The characterization study of those materials in terms of C compositions and functional groups is shown in Figs. S6 and S7, and Table S2 and the details are described in Text S4. In brief, the contents of oxidative groups such as C═O and COO^- was found to be increased with Oxi-R550, i.e., the former group increased from 3.03 to 5.99% and the latter group increased from 5.38 to 8.16%, while the increase of the relative proportion of C—O was observed from 16.75 to 24.35%, with the H-R550 sample. As a result, the Oxi-R550, with the highest percentage of COO^- among the three kinds of biochars, showed a maximum degradation of PNP in the Oxi-R550 added S(IV)-Cr(VI) system. As shown in Figs. 4a and S8a, upon the addition of Oxi-R550 into the S(IV)-Cr(VI) system, the degradation of PNP was promoted by 27.2%, i.e. from 20.9 to 48.1% at a period of 60 min. The degradation of PNP with the solo Oxi-R550 system was observed to be 0. As shown in Figs. 1a, 4a, and S8d, the degradation of PNP with the R550-S(IV)-Cr(VI) and H-R550-S(IV)-Cr(VI) systems, was found to be increased to 56.1% and 43.2%, respectively at a period of 60 min. If the degradation contribution of R550 (10.67%) and H-R550 (29.14%) samples caused

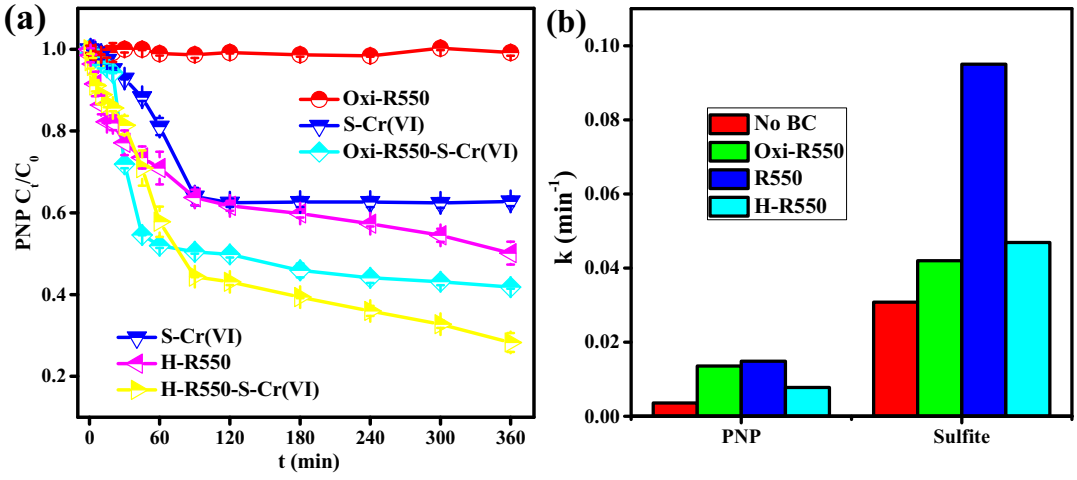

Fig. 4. (a) Oxi-R550 and H-R550 was enhancing the degradation of PNP in the coexisted S(IV)-Cr(VI) system. (b) Comparison of PNP degradation and sulfite removal kinetics (simulated with first-order kinetic model) in the S(IV)-Cr(VI) system as Oxi-R550, R550, and H-R550 coexisted. Reaction conditions: $[PNP]_0 = 0.04$ mM, $[Cr(VI)]_0 = 0.2$ mM, $[sulfite]_0 = 5$ mM, $[Biochar]_0 = 1$ g L^{-1}, pHini = 7.

by the activation of O_2, were excluded, the respective obtained promotion of PNP degradation is 24.53% and −6.84%, which is an evidence for the enhancement of COO^- of biochar towards the S(IV)-Cr(VI) reaction.

The COO^- of biochar not only improved the activation of sulfite by Cr(VI) (Reactions 16 and 17) but suppressing the possibility of the side reactions (Reactions 10 and 11), which favors sulfite oxidization step. Hence, the quick decomposition of sulfite is not necessarily to be a cause for the promoted degradation of PNP, wherein the high-efficiency of SO_3^{2-} to $SO_4^{\bullet-}$ conversion was crucial. As shown in Fig. 4b, the decay constant of sulfite in the simple S(IV)-Cr(VI) system was 0.0308 min^{-1} and it was increased to 1.36 times higher of 0.042, 1.52 times higher of 0.095 and 2.94 times higher of 0.0469 min^{-1} for Oxi-R550-S(IV)-Cr(VI), R550-S(IV)-Cr(VI) and H-R550-S(IV)-Cr(VI) systems, respectively. In the meantime, the constant of PNP degradation was 0.0036 min^{-1} in the simple S(IV)-Cr(VI) system and it was increased to 0.0136, 0.0149, and 0.0078 min^{-1} with Oxi-R550, R550, and H-R550, added S(IV)-Cr(VI) systems, respectively. Excluding the contribution of the activation of O_2 via the biochar, the degradation rate of PNP was promoted by 2.78, 2.67 and 0 times with the three kinds of biochars added S(IV)-Cr(VI) system, respectively. Thus, the Oxi-R550, with the least enhancement on the oxidization of sulfite by Cr(VI), accelerated the PNP degradation to a higher extent. These results suggest that the COO^- of biochar not only enhances the activation of sulfite by Cr(VI) but also improves the conversion of SO_3^{2-} to $SO_4^{\bullet-}$ by suppressing the undesirable side reactions of sulfite transformation.

As shown in Fig. 5a and b, and Table 2, the C compositions of Oxi-R550, after the degradation process, hardly changed, which is consistent with its poor performance of activation of O_2. However, in the Oxi-R550-S(IV)-Cr(VI) system, the relative percentage of COO^- observed with sole Oxi-R550 (8.16%), was dramatically decreased to 3.67% (Fig. 5c and Table 2), along with a decline of C/Si ratio from 11.99 to 10.73. Such a result confirmed the decline of COO^- on biochar upon the S(IV)-Cr(VI) reaction, consistent with the change of COO^- on biochar R550. As speculated in the earlier discussion, COO^- could be removed from the biochar after forming a complex with Cr(VI). Such removal of COO^- resulted in a significant increase of C-C/C=C from 69.71 to 73.33%, a slight raise of C—O from 16.14 to 16.64%, as well as C=O from 5.99 to 6.36%. The influence of biochar COO^- in the S(IV)-Cr(VI) reaction was further confirmed.

Table 2
C composition for Oxi-R550 and H-R550 based on XPS Analysis after PNP degradation in the absence and presence of S(IV)-Cr(VI) reaction. Reaction conditions: $[PNP]_0 = 0.04$ mM, $[Cr(VI)]_0 = 0.2$ mM, $[sulfite]_0 = 5$ mM, $[Biochar]_0 = 1$ g L^{-1}, pHini = 7.

System	C/Si	O/Si	C-C/C=C	C-O	C=O	COO^-
Oxi-R550	11.99	3.44	69.71%	16.14%	5.99%	8.16%
Oxi-R550-PNP	12.20	3.34	69.24%	16.31%	6.12%	8.33%
Oxi-R550-S-Cr-PNP	10.73	2.95	73.33%	16.64%	6.36%	3.67%
H-R550	11.96	2.66	64.06%	24.35%	7.14%	4.45%
H-R550-PNP	12.31	2.74	63.59%	21.72%	8.51%	6.18%
H-R550-S-Cr-PNP	12.07	2.87	63.54%	20.08%	9.30%	7.08%

As seen in Fig. 5d-f and Table 2, the C composition of H-R550 was varied during the degradation reaction with and without the S(IV)-Cr(VI). After the degradation, the relative percentage of C—O of H-R550 was notably decreased from 24.35 to 21.72% with sole H-R550 and the decrease was further down to 20.08% with H-R550-S(IV)-Cr(VI) system. At the same time, the increase of C=O and COO^- was seen from 7.14 to 8.51% and from 4.45 to 6.18%, respectively, and it was further hiked to an extent of 9.30 and 7.08% with H-R550-S(IV)-Cr(VI) system. The variations demonstrated that the S(IV)-Cr(VI) reaction enhanced the oxidization level of H-R550. Besides, the decline of COO^- and increase of C-C/C=C owing to an enhancement of the S(IV)-Cr(VI) reaction was not observed in the H-R550-S(IV)-Cr(VI) system, which is in accordance with its insignificant contribution observed towards the PNP degradation in the S(IV)-Cr(VI) system. It was originated from the least content of COO^- of H-R550.

3.5. Impact of defect of biochar on S(IV)-Cr(VI) reaction and PNP degradation

The defective sites presented on the biochar might also influence the rate of PNP degradation in the biochar added S(IV)-Cr(VI) system. The

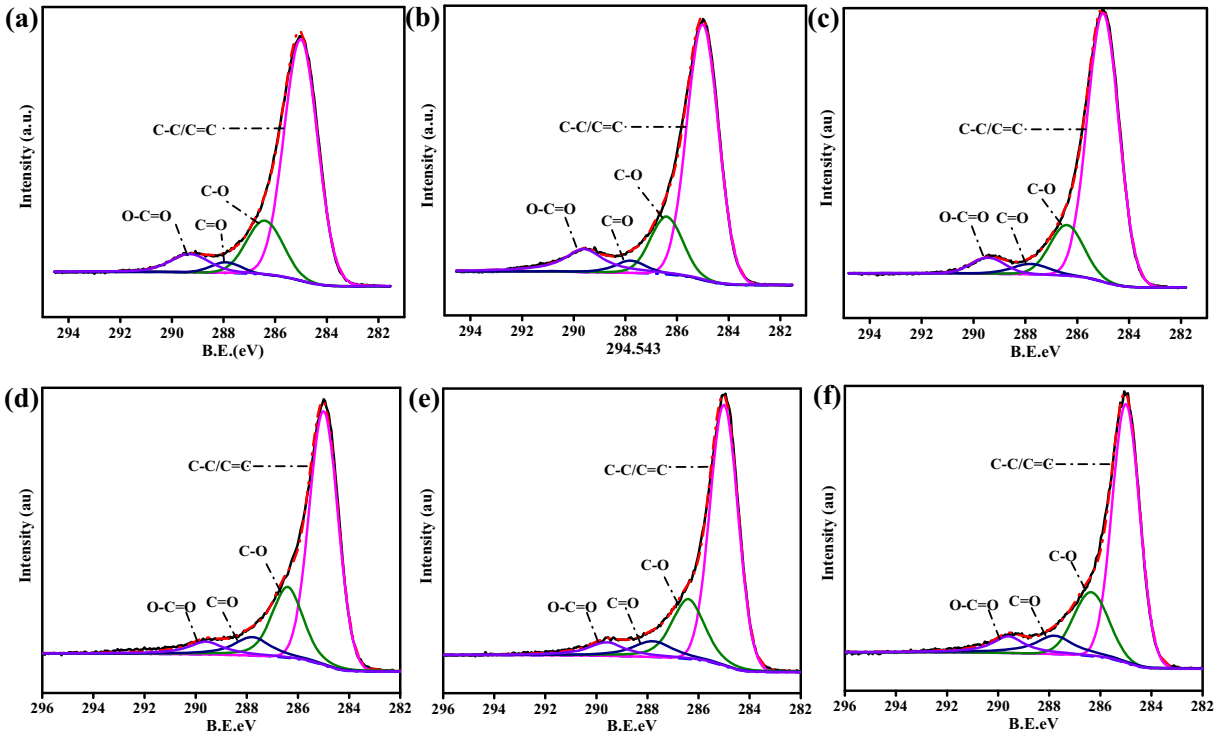

Fig. 5. C 1s XPS spectra of biochar (a for Oxi-R550, d for H-R550) before and after PNP degradation in the absence (b for Oxi-R550, e for H-R550) and presence (c for Oxi-R550, f for H-R550) of S(IV)-Cr(VI) reaction. Reaction conditions: $[PNP]_0 = 0.04$ mM, $[Cr(VI)]_0 = 0.2$ mM, $[sulfite]_0 = 5$ mM, $[Biochar]_0 = 1$ g L^{-1}, pHini = 7.

R800, having a high level of the defect and less content of COO^- (Zhang et al., 2019a). The defective level of biochar could be assessed by the I_D/I_G ratio in the Raman spectra (Fig. S10), which was 0.963 for R800, higher than 0.751 of R550 and 0.718 for Oxi-R550. Such a result demonstrated the high defective level of R800. Then R800 was introduced into the S(IV)-Cr(VI) system. As shown in Fig. S11, the degradation of PNP was promoted from 11.8 to 44.5% at 45 min, by the influence of R800 in the R800-S(IV)-Cr(VI) system. The degradation of PNP was enhanced only by 14.5%, considering the degradation of 18.2% with the solo R800 system, which was lower than the 27.2% observed with the Oxi-R550 system. The defective sites presented on biochar were not a key factor in enhancing the PNP degradation in the biochar-S(IV)-Cr(VI) system.

3.6. Analysis of PNP degradation intermediates

The intermediates formed during the degradation of PNP were investigated in the S(IV)-Cr(VI) system with and without R550. The usual intermediates such as phenol, p-benzoquinone, and maleic acid, were detected, which confirms the radical degradation pathway of PNP by the conventional ROS viz. •OH and SO_4•$^-$ (Chen et al., 2016) in both the systems. The existing period of the intermediates of higher concentration confirms that the decreased PNP was initially oxidized into phenol, followed by benzoquinone and maleic acid, and then finally mineralized into CO_2 and H_2O. As shown in Fig. 6a, the maximum concentration of phenol (5.47 μM) was detected at a reaction period of 20 min, and it was at 45 min, for benzoquinone (0.11 μM) and maleic acid (8.33 μM).

Because the R550 accelerated the activation of sulfite by Cr(VI) which produces ROS in large quantity, thereby the higher degradation of PNP as well as the faster transformation of the intermediates. As shown in Fig. 6b, in the R550-S(IV)-Cr(VI) system, a maximum concentration of phenol (10.15 μM), benzoquinone (0.14 μM) and maleic acid (4.87 μM) was detected at 10, 20 and 30 min, respectively, which are in advance to that of those in the sole S(IV)-Cr(VI) system. It demonstrates the quick transformation of the PNP molecule with the R550 added S(IV)-Cr(VI) system.

3.7. Effect of the dosages of sulfite, Cr(VI) and biochar on PNP degradation

The effect of the dosage of sulfite, Cr(VI), and biochar on PNP degradation was studied in view of practical applications. As shown in Fig. S12, a, d, and g, at a reaction period of 90 min, the degradation of PNP was 27.2, 36.1, and 33.4% for the sulfite dosage of 2, 5, and 10 mM, respectively. However, the Cr(VI) was reduced only to an extent of 83.3% with the sulfite dosage of 2 mM and a total reduction was observed with the dosages of 5 and 10 mM (Fig. S12b, e, and h). On the other hand, 0.2 mM of Cr(VI) consumed the entire sulfite content of 2 and 5 mM dosages, and only 42% content of the 10 mM dosage (Fig. S12c, f and i). Based on this, an optimum dosage sulfite and Cr (VI) was fixed as 5 mM and 0.2 mM, respectively.

The degradation efficiency of PNP was increased with the concentration of Cr(VI) at neutral pH conditions. As shown in Fig. S13 a, d and e, at a reaction period of 90 min in the system containing 5 mM of sulfite, the degradation of PNP was found to be progressively increased as 19.1, 36.0 and 56.5% with the Cr(VI) addition of 0.1, 0.2 and 0.4 mM, respectively, and upon the addition of R550 into each system, the respective degradation efficiency was promoted to 27, 59 and 56.6%. The enhanced degradation was mostly due to the acceleration of sulfite activation by the increasing dosage of Cr(VI), which could be confirmed by the increasing consumption of sulfite. As shown in Fig. S13 c, f, and i, at a reaction period of 90 min, the efficiency of sulfite consumption was significantly increased from 44.1 to 100% with increased addition of Cr (VI) from 0.1 to 0.4 mM, respectively. However, in the 0.4 mM of Cr (VI) with R550, the influence of R550 on the reactions of Cr(VI) activating sulfite as well as PNP degradation was negligible, probably due to an effective reaction between Cr(IV) and sulfite, which could overcome the activity of R550.

Biochar as a higher dosage could lead to better PNP degradation and faster reaction between Cr(VI) and sulfite. As shown in Fig. 7a, biochar at a low dosage functioned a poor performance towards PNP degradation. Only 6.4% of PNP (0.04 mM) could be degraded within 360 min by 0.2 g L^{-1} of R550. As the biochar R550 dosage increased to 1 g L^{-1}, the PNP degradation efficiency within 360 min was raised to 36.6%. As for the S(IV)-Cr(VI) system, the enhancement of PNP degradation, Cr (VI) reduction, and sulfite oxidization was correlated with the dosage of biochar in this study. Fig. 7a exhibited the PNP degradation in the biochar R550-S(IV)-Cr(VI) systems with the biochar dosage varying from 0.2 to 1 g L^{-1}. As the biochar R550 absented, 36.1% of PNP was degraded within 90 min in the S(IV)-Cr(VI) system. And the degradation efficiency of PNP was promoted to 41.3%, 46.3%, and 59%, respectively, as 0.2, 0.5, and 1 g L^{-1} of biochar was introduced into the system. Such a result demonstrated the promotion of PNP degradation caused by biochar in the S(IV)-Cr(VI) system. Meanwhile, the accelerated removal of Cr(VI) and sulfite could be attained owing to the presence of biochar R550. As shown in Fig. 7b, the period for completely removing Cr(VI) was reduced from the original 120 min to shorter periods of 90, 60 and 45 min with increasing the biochar dosage to 0.2, 0.5, and 1 g L^{-1}, respectively. Fig. 7c described the faster sulfite oxidization in the S

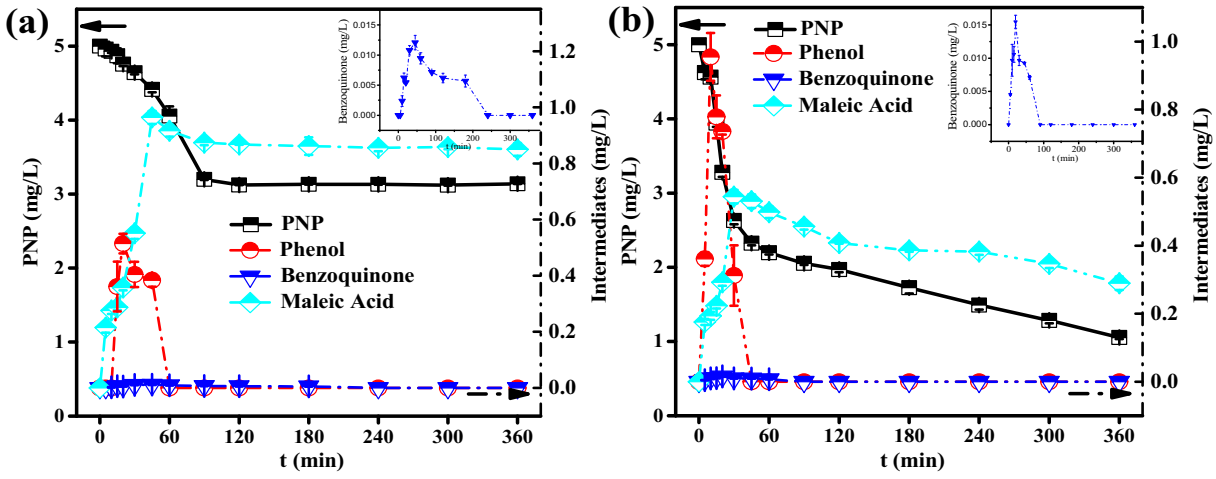

Fig. 6. Intermediates of PNP degradation in the S(IV)-Cr(VI) system with R550 absence (a) and presence (b). Reaction conditions: $[PNP]_0 = 0.04$ mM, $[Cr(VI)]_0 = 0.2$ mM, $[sulfite]_0 = 5$ mM, $[Biochar]_0 = 1$ g L^{-1}, pHini = 7.

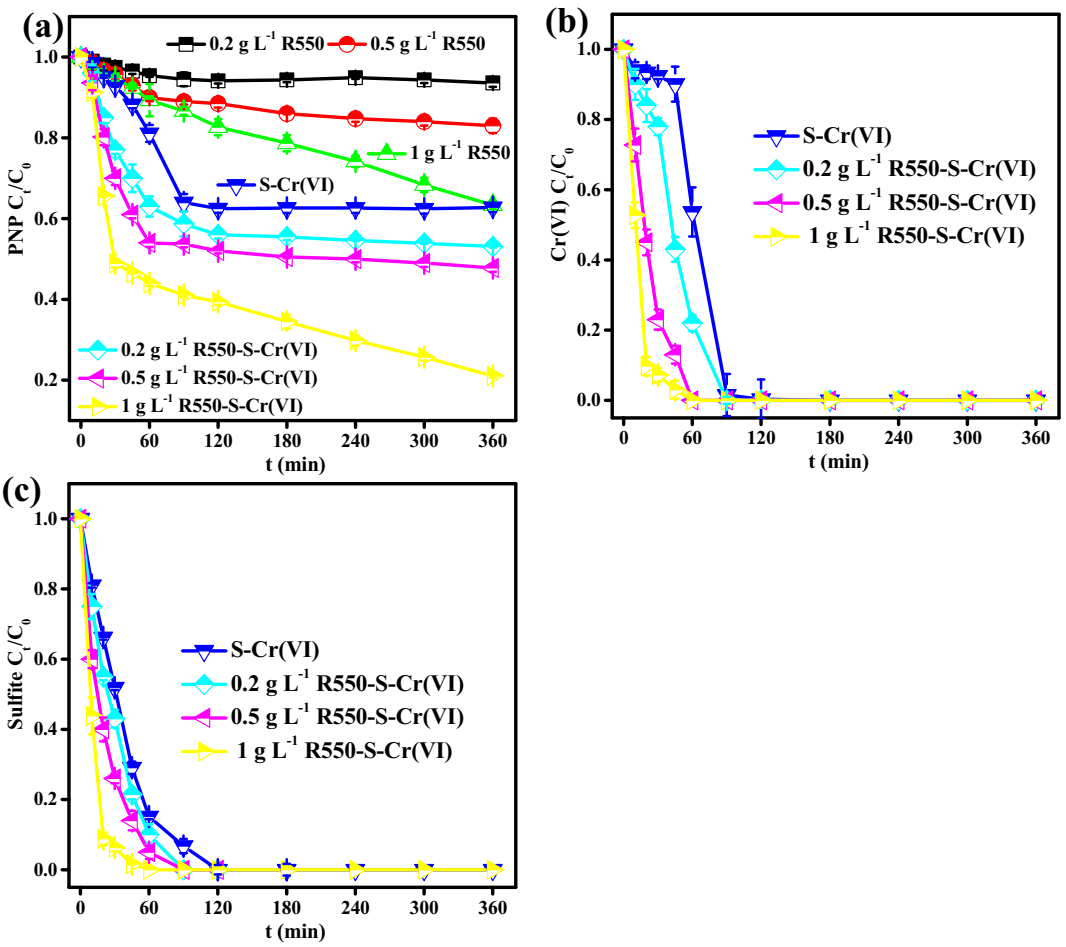

Fig. 7. Effects of biochar dosage on the reaction of Cr(VI) activating sulfite and PNP degradation in S(IV)-Cr(VI) system as R550 presented. (a), (b) and (c) were for PNP degradation, Cr(VI) removal and sulfite oxidization, respectively. Reaction condition: $[PNP]_0 = 0.04$ mM, $[sulfite]_0 = 5$ mM, $[Cr(VI)]_0 = 0.2$ mM, pHini = 7, the dosage of biochar R550 varied from 0.2 to 1 g L^{-1}.

(IV)-Cr(VI) system because of the introduction of biochar R550. The removal efficiency of sulfite within 60 min was evaluated from the original 84.9% to 100% with the biochar dosage increasing from 0 to 1 g L^{-1}. Such a phenomenon about the faster removal of Cr(VI) and sulfite demonstrated the biochar's capacity to accelerate the S(IV)-Cr(VI) reaction, thus resulting in the production of reactive oxygen species at higher content and the enhanced degradation of PNP.

3.8. Stability and reusability of R550 in the S(IV)-Cr(VI) system and PNP degradation

Biochar R550 displayed poor stability and reusability on enhancing the S(IV)-Cr(VI) reaction and PNP degradation. As shown in Fig. 8a, the degradation efficiency of PNP in the R550-S(IV)-Cr(VI) system within 30 min was 51.1% as the biochar R550 was first used, while it decreased to 42.8% and 33.9% as the biochar R550 was second and third used. Such a decline in PNP degradation was owing to the alleviated reaction between sulfite and Cr(VI), which could be verified in Fig. 8b and c. As the biochar R550 was first used in the S(IV)-Cr(VI) system, 47.3% of Cr(VI) was removed within 10 min, while it decreased to 36.6% and 25.5% (Fig. 8b) in the second and third cycles, respectively. Similar results could also be attained in the sulfite removal. As the R550 cycle increased to 3 times, the removal efficiency of sulfite within 10 min decreased from 56.2% to 37% (Fig. 8c). These results could be ascribed to the diminishment of COO^- on biochar upon the S(IV)-Cr(VI) reaction, which resulted in the decreasing complex formation with Cr(VI), the declined reactivity of Cr(VI) and slow activation of sulfite, finally resulting in the decline of PNP degradation.

After its fast degradation within 30 mins, the slow degradation of PNP proceeded. However, with increasing the biochar cycle to 3 times, the degradation efficiency in the period from 30 to 360 min decreased from 27.8% to 14.8%. The slow degradation of PNP was mainly originated from the •OH production from serial reactions of O_2 reduction by biochar. With increasing the biochar cycle, the oxidization of biochar occurred gradually, thus the sluggish O_2 activation and PNP degradation came out.

4. Conclusions

Developing a process for Cr(VI) reduction with sulfite ions is a novel approach for the decontamination of the aqueous system containing multiple pollutants of Cr(VI) and toxic organic compounds. However, the working pH suggested for this process is highly acidic (usually pH 2–3) and then an alkali is mandatory for precipitating the Cr in the subsequent stage. Also, the refractory organic pollutants are hardly degraded in the system. The present study reports the beneficial influence of biochar on the reduction of Cr(VI) with sulfite ions as well as on the degradation of coexisting organic pollutants at neutral pH conditions. It was found that the carboxyl on biochar efficiently enhanced the reactivity of Cr(VI) via coordination, then accelerated the reduction of Cr(VI) by sulfite. Such coordination also promoted the activation of sulfite by Cr(VI) to produce ROS (SO_4•$^-$ and •OH) and contributed to the radical

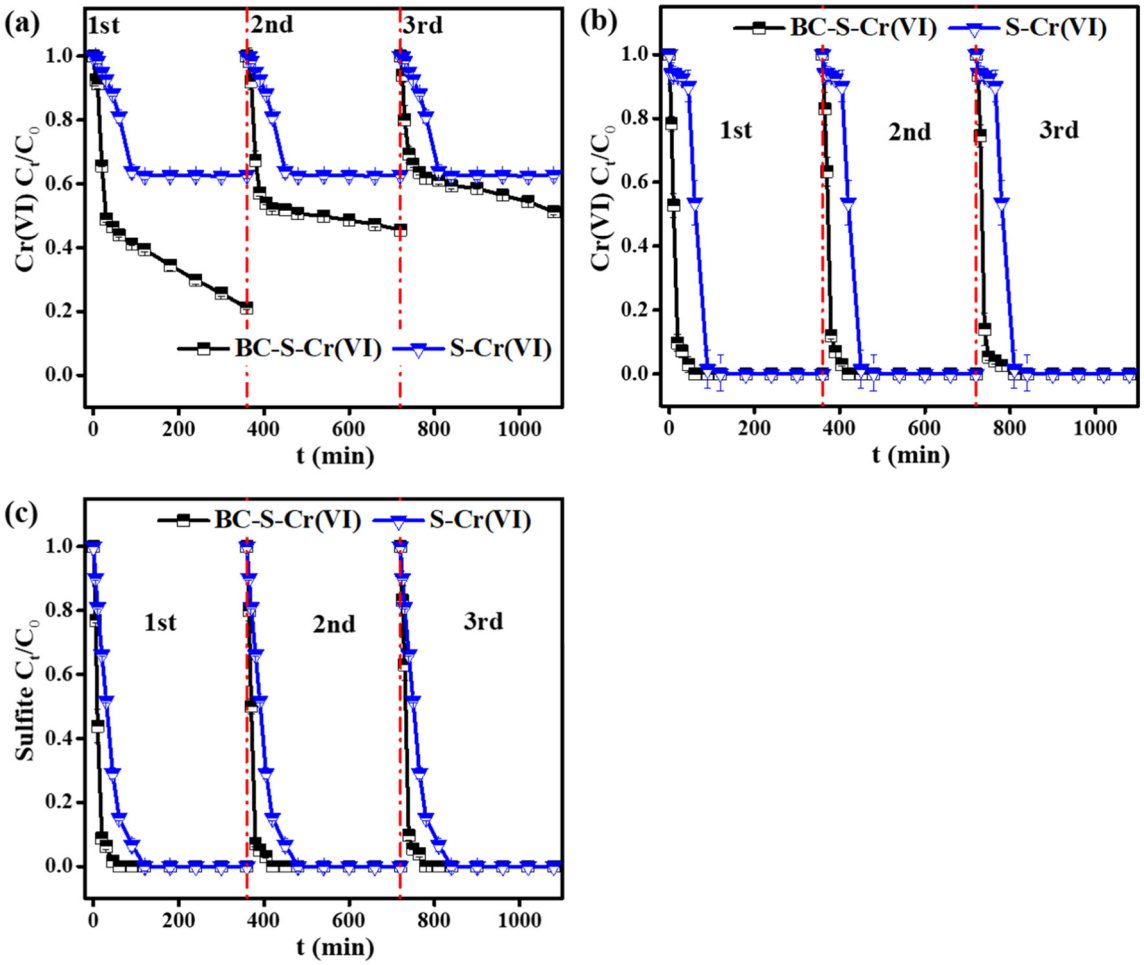

Fig. 8. PNP degradation (a) Cr(VI) removal (b) and sulfite oxidization (c) in the S(IV)-Cr(VI) system using the recycled R550. Reaction conditions: $[PNP]_0 = 0.04$ mM, $[Cr(VI)]_0 = 0.2$ mM, $[sulfite]_0 = 5$ mM, $[Biochar]_0 = 1$ g L^{-1}, pHini = 7.

degradation of coexisted PNP. Besides, the coordination between Cr(VI) and biochar inhibited the side reactions of $CrSO_6^{2-}$ reacting with $HCrO_4^-$ to produce $O_3CrOCrO_3SO_3^{2-}$ that did not contribute to the generation of $SO_4^{\bullet-}$. Moreover, biochar, a cost-effective by-product of the biowaste recycling process, could be produced and employed on a large-scale. Further, no external energy and adding oxidants (e.g., H_2O_2 and O_3) are needed. Hence, the addition of biochar and sulfite into the industrial wastewaters containing Cr(VI) and organic pollutants, is highly viable and feasible.

CRediT authorship contribution statement

Kaikai Zhang: Conceptualization, Methodology, Writing - original draft, Validation, Formal analysis, Investigation, Data curation, Visualization. **Peng Sun:** Software, Validation. **Yu Zhang:** Resources. **Muthu Murugananthan:** Writing - review & editing. **Kumaravel Ammasai:** Writing - review & editing. **Yanrong Zhang:** Supervision, Project administration, Funding acquisition.

Declaration of competing interest

We declare that we have no financial and personal relationships with other people or organizations that can inappropriately influence our work, there is no professional or other personal interest of any nature or kind in any product, service and/or company that could be construed as influencing the position presented in, or the review of, the manuscript entitled "Enhancement of S(IV)-Cr(VI) reaction in p-nitrophenol degradation using rice husk biochar at neutral conditions".

Acknowledgment

This work was supported by the International Science & Technology Cooperation Program of China (Nos. 2013DFG50150 and 2016YFE0126300) and the Innovative and Interdisciplinary Team at HUST (2015ZDTD027). The authors thank the Analytical and Testing Center of HUST for the use of FTIR, XRD, and XPS equipment.

Appendix A. Supplementary data

Supplementary data to this article can be found online at https://doi.org/10.1016/j.scitotenv.2020.142086.

References

Cao, F., Liu, H., Wu, F., Lu, S., 2016. Automated determination of chromium (VI) in tannery effluent using flow injection analysis with an optical flow cell and detector. Water Air Soil Pollut. 228. https://doi.org/10.1007/s11270-016-3162-y.

Chen, T., Zhou, Z., Xu, S., Wang, H., Lu, W., 2015. Adsorption behavior comparison of trivalent and hexavalent chromium on biochar derived from municipal sludge. Bioresour. Technol. 190, 388–394. https://doi.org/10.1016/j.biortech.2015.04.115.

Chen, X., Murugananthan, M., Zhang, Y., 2016. Degradation of p-Nitrophenol by thermally activated persulfate in soil system. Chem. Eng. J. 283, 1357–1365. https://doi.org/10.1016/j.cej. 2015.08.107.

Das, P., Mondal, G.C., Singh, S., Singh, A.K., Prasad, B., Singh, K.K., 2018. Effluent treatment technologies in the iron and steel industry - a state of the art review. Water Environ. Res. 90, 395–408. https://doi.org/10.2175/106143017X15131012152951.

Davoudi, M., Gholami, M., Naseri, S., Mahvi, A.H., Farzadkia, M., Esrafili, A., et al., 2014. Application of electrochemical reactor divided by cellulosic membrane for optimized simultaneous removal of phenols, chromium, and ammonia from tannery effluents. Toxicol. Environ. Chem. 96, 1310–1332. https://doi.org/10.1080/02772248.2014.942311.

Diao, Z.H., Du, J.J., Jiang, D., Kong, L.J., Huo, W.Y., Liu, C.M., et al., 2018. Insights into the simultaneous removal of Cr(6+) and Pb(2+) by a novel sewage sludge-derived biochar immobilized nanoscale zero valent iron: coexistence effect and mechanism. Sci. Total Environ. 642, 505–515. https://doi.org/10.1016/j.scitotenv.2018.06.093.

Ding, L., Zhang, P., Luo, H., Hu, Y., Norouzi Banis, M., Yuan, X., et al., 2018. Nitrogen-doped carbon materials as metal-free catalyst for the dechlorination of trichloroethylene by sulfide. Environ. Sci. Technol. 52, 14286–14293. https://doi.org/10.1021/acs.est.8b03565.

Dong, X., Ma, L.Q., Gress, J., Harris, W., Li, Y., 2014. Enhanced Cr(VI) reduction and As(III) oxidation in ice phase: important role of dissolved organic matter from biochar. J. Hazard. Mater. 267, 62–70. https://doi.org/10.1016/j.jhazmat.2013.12.027.

Dong, H., Wei, G., Cao, T., Shao, B., Guan, X., Strathmann, T.J., 2020. Insights into the oxidation of organic cocontaminants during Cr(VI) reduction by sulfite: the overlooked significance of Cr(V). Environ. Sci. Technol. 54, 1157–1166. https://doi.org/10.1021/acs.est.9b03356.

Du, J., Guo, W., Wang, H., Yin, R., Zheng, H., Feng, X., et al., 2017. Hydroxyl radical dominated degradation of aquatic sulfamethoxazole by Fe^0/bisulfite/O_2: kinetics, mechanisms, and pathways. Water Res. 138, 323–332. https://doi.org/10.1016/j.watres.2017.12.046.

Duan, X., Sun, H., Tade, M., Wang, S., 2018. Metal-free activation of persulfate by cubic mesoporous carbons for catalytic oxidation via radical and nonradical processes. Catal. Today 307, 140–146. https://doi.org/10.1016/j.cattod.2017.04.038.

Fang, G., Gao, J., Liu, C., Dionysiou, D.D., Wang, Y., Zhou, D., 2014. Key role of persistent free radicals in hydrogen peroxide activation by biochar: implications to organic contaminant degradation. Environ. Sci. Technol. 48, 1902–1910. https://doi.org/10.1021/es4048126.

Fang, G., Liu, C., Gao, J., Dionysiou, D.D., Zhou, D., 2015a. Manipulation of persistent free radicals in biochar to activate persulfate for contaminant degradation. Environ. Sci. Technol. 49, 5645–5653. https://doi.org/10.1021/es5061512.

Fang, G., Zhu, C., Dionysiou, D.D., Gao, J., Zhou, D., 2015b. Mechanism of hydroxyl radical generation from biochar suspensions: implications to diethyl phthalate degradation. Bioresour. Technol. 176, 210–217. https://doi.org/10.1016/j.biortech.2014.11.032.

Fang, G., Liu, C., Wang, Y., Dionysiou, D.D., Zhou, D., 2017. Photogeneration of reactive oxygen species from biochar suspension for diethyl phthalate degradation. Appl. Catal. B 214, 34–45. https://doi.org/10.1016/j.apcatb.2017.05.036.

Gil-Cardeza, M.L., Ferri, A., Cornejo, P., Gomez, E., 2014. Distribution of chromium species in a Cr-polluted soil: presence of Cr(III) in glomalin related protein fraction. Sci. Total Environ. 493, 828–833. https://doi.org/10.1016/j.scitotenv.2014.06.080.

Gu, Y., Dong, W., Luo, C., Liu, T., 2016. Efficient reductive decomposition of perfluorooctanesulfonate in a high photon flux UV/sulfite system. Environ. Sci. Technol. 50, 10554–10561. https://doi.org/10.1021/acs.est.6b03261.

Habibul, N., Hu, Y., Wang, Y.K., Chen, W., Yu, H.Q., Sheng, G.P., 2016. Bioelectrochemical chromium(VI) removal in plant-microbial fuel cells. Environ. Sci. Technol 50, 3882–3889. https://doi.org/10.1021/acs.est.5b06376.

Hu, S., Zhang, D., Yang, Y., Ran, Y., Mao, J., Chu, W., et al., 2019. Effects of the chemical structure, surface, and micropore properties of activated and oxidized black carbon on the sorption and desorption of phenanthrene. Environ. Sci. Technol. 53, 7683–7693. https://doi.org/10.1021/acs.est.9b01788.

Jiang, D., Li, Y., Wu, Y., Zhou, P., Lan, Y., Zhou, L., 2012. Photocatalytic reduction of Cr(VI) by small molecular weight organic acids over schwertmannite. Chemosphere 89, 832–837. https://doi.org/10.1016/j.chemosphere.2012.05.001.

Jiang, W., Cai, Q., Xu, W., Yang, M., Cai, Y., Dionysiou, D.D., et al., 2014. Cr(VI) adsorption and reduction by humic acid coated on magnetite. Environ. Sci. Technol. 48, 8078–8085. https://doi.org/10.1021/es405804m.

Jiang, B., Liu, Y., Zheng, J., Tan, M., Wang, Z., Wu, M., 2015. Synergetic transformations of multiple pollutants driven by Cr(VI)-sulfite reactions. Environ. Sci. Technol. 49, 12363–12371. https://doi.org/10.1021/acs.est.5b03275.

Jiang, B., Wang, X., Liu, Y., Wang, Z., Zheng, J., Wu, M., 2016. The roles of polycarboxylates in Cr(VI)/sulfite reaction system: involvement of reactive oxygen species and intramolecular electron transfer. J. Hazard. Mater. 304, 457–466. https://doi.org/10.1016/j.jhazmat.2015.11.011.

Jiang, B., He, H., Liu, Y., Tang, Y., Luo, S., Wang, Z., 2018. pH-dependent roles of polycarboxylates in electron transfer between Cr(VI) and weak electron donors. Chemosphere 197, 367–374. https://doi.org/10.1016/j.chemosphere.2018.01.047.

Kang, J., Duan, X., Wang, C., Sun, H., Tan, X., Tade, M.O., et al., 2018. Nitrogen-doped bamboo-like carbon nanotubes with Ni encapsulation for persulfate activation to remove emerging contaminants with excellent catalytic stability. Chem. Eng. J. 332, 398–408. https://doi.org/10.1016/j.cej.2017.09.102.

Li, X., Ma, J., Liu, G., Fang, J., Yue, S., Guan, Y., et al., 2012. Efficient reductive dechlorination of monochloroacetic acid by sulfite/UV process. Environ. Sci. Technol 46, 7342–7349. https://doi.org/10.1021/es3008535.

Liu, J., Huang, K., Xie, K., Yang, Y., Liu, H., 2016. An ecological new approach for treating Cr (VI)-containing industrial wastewater: photochemical reduction. Water Res. 93, 187–194. https://doi.org/10.1016/j.watres.2016.02.025.

Liu, Z., Yang, S., Yuan, Y., Xu, J., Zhu, Y., Li, J., et al., 2017. A novel heterogeneous system for sulfate radical generation through sulfite activation on a $CoFe_2O_4$ nanocatalyst surface. J. Hazard. Mater. 324, 583–592. https://doi.org/10.1016/j.jhazmat.2016.11.029.

Liu, Q., Liggio, J., Li, K., Lee, P., Li, S.M., 2019. Understanding the impact of relative humidity and coexisting soluble iron on the OH-initiated heterogeneous oxidation of organophosphate flame retardants. Environ. Sci. Technol. 53, 6794–6803. https://doi.org/10.1021/acs.est.9b01758.

Lu, L., Chen, B., 2018. Enhanced bisphenol A removal from stormwater in biochar-amended biofilters: combined with batch sorption and fixed-bed column studies. Environ. Pollut. 243, 1539–1549. https://doi.org/10.1016/j.envpol.2018.09.097.

Mytych, P., Stasicka, Z., 2004. Photochemical reduction of chromium(VI) by phenol and its halogen derivatives. Appl. Catal. B 52, 167–172. https://doi.org/10.1016/j.apcatb.2004.04. 006.

Oh, S.Y., Chu, D., Chiu, P.C., 2002. Graphite-mediated reduction of 2,4-dinitrotoluene with elemental iron. Environ. Sci. Technol. 36, 2178–2184. https://doi.org/10.1021/es011474g.

Oh, S.Y., Son, J.G., Lim, O.T., Chiu, P.C., 2012. The role of black carbon as a catalyst for environmental redox transformation. Environ. Geochem. Health 34 (Suppl. 1), 105–113. https://doi.org/10.1007/s10653-011-9416-0.

Rivero-Huguet, M., Marshall, W.D., 2009. Influence of various organic molecules on the reduction of hexavalent chromium mediated by zero-valent iron. Chemosphere 76, 1240–1248. https://doi.org/10.1016/j.chemosphere.2009.05.040.

Shakir, L., Ejaz, S., Ashraf, M., Ahmad, N., Javeed, A., 2012. Characterization of tannery effluent wastewater by proton-induced X-ray emission (PIXE) analysis to investigate their role in water pollution. Environ. Sci. Pollut. Res. Int. 19, 492–501. https://doi.org/10.1007/s11356-011-0586-1.

Szpyrkowicz, L., Kaul, S.N., Neti, R.N., Satyanarayan, S., 2005. Influence of anode material on electrochemical oxidation for the treatment of tannery wastewater. Water Res. 39, 1601–1613. https://doi.org/10.1016/j.watres.2005.01.016.

Teixido, M., Hurtado, C., Pignatello, J.J., Beltran, J.L., Granados, M., Peccia, J., 2013. Predicting contaminant adsorption in black carbon (biochar)-amended soil for the veterinary antimicrobial sulfamethazine. Environ. Sci. Technol. 47, 6197–6205. https://doi.org/10.1021/es400911c.

Wang, Q., Chen, X., Yu, K., Zhang, Y., Cong, Y., 2013. Synergistic photosensitized removal of Cr(VI) and Rhodamine B dye on amorphous TiO_2 under visible light irradiation. J. Hazard. Mater. 246–247, 135–144. https://doi.org/10.1016/j.jhazmat.2012.12.017.

Wang, S., Li, L., Zhu, Z., Zhao, M., Zhang, L., Zhang, N., et al., 2019. Remarkable improvement in photocatalytic performance for tannery wastewater processing via SnS_2 modified with N-doped carbon quantum dots: synthesis, characterization, and 4-nitrophenol-aided Cr(VI) photoreduction. Small 15, e1804515. https://doi.org/10.1002/small. 201804515.

Xiao, X., Chen, B., Zhu, L., 2014. Transformation, morphology, and dissolution of silicon and carbon in rice straw-derived biochars under different pyrolytic temperatures. Environ. Sci. Technol. 48, 3411–3419. https://doi.org/10.1021/es405676h.

Xie, P., Zhang, L., Chen, J., Ding, J., Wan, Y., Wang, S., et al., 2019. Enhanced degradation of organic contaminants by zero-valent iron/sulfite process under simulated sunlight irradiation. Water Res. 149, 169–178. https://doi.org/10.1016/j.watres.2018.10.078.

Xu, J., Ding, W., Wu, F., Mailhot, G., Zhou, D., Hanna, K., 2016a. Rapid catalytic oxidation of arsenite to arsenate in an iron(III)/sulfite system under visible light. Appl. Catal. B 186, 56–61. https://doi.org/10.1016/j.apcatb.2015.12.033.

Xu, S., Adhikari, D., Huang, R., Zhang, H., Tang, Y., Roden, E., et al., 2016b. Biochar-facilitated microbial reduction of hematite. Environ. Sci. Technol 50, 2389–2395. https://doi.org/10.1021/acs.est.8b03565.

Xu, X., Huang, H., Zhang, Y., Xu, Z., Cao, X., 2019. Biochar as both electron donor and electron shuttle for the reduction transformation of Cr(VI) during its sorption. Environ. Pollut. 244, 423–430. https://doi.org/10.1016/j.envpol.2018.10.068.

Yuan, Y., Yang, S., Zhou, D., Wu, F., 2016. A simple Cr(VI)-S(IV)-O_2 system for rapid and simultaneous reduction of Cr(VI) and oxidative degradation of organic pollutants. J. Hazard. Mater. 307, 294–301. https://doi.org/10.1016/j.jhazmat.2016.01.012.

Zewdu, F., Amare, M., Wong, B.M., 2018. Determination of the level of hexavalent, trivalent, and total chromium in the discharged effluent of Bahir Dar tannery using ICP-OES and UV–visible spectrometry. Cogent Chem 4, 1534566. https://doi.org/10.1080/23312009. 2018.1534566.

Zhang, W., Zheng, J., Zheng, P., Qiu, R., 2015. Atrazine immobilization on sludge derived biochar and the interactive influence of coexisting Pb(II) or Cr(VI) ions. Chemosphere 134, 438–445. https://doi.org/10.1016/j.chemosphere.2015.05.011.

Zhang, Y., Wang, Q., Lu, J., Wang, Q., Cong, Y., 2016. Synergistic photoelectrochemical reduction of Cr(VI) and oxidation of organic pollutants by g-C_3N_4/TiO_2-NTs electrodes. Chemosphere 162, 55–63. https://doi.org/10.1016/j.chemosphere.2016.07.064.

Zhang, J., Zhu, L., Shi, Z., Gao, Y., 2017. Rapid removal of organic pollutants by activation sulfite with ferrate. Chemosphere 186, 576–579. https://doi.org/10.1016/j.chemosphere.2017.07. 102.

Zhang, J., Ma, J., Song, H., Sun, S., Zhang, Z., Yang, T., 2018a. Organic contaminants degradation from the S(IV) autoxidation process catalyzed by ferrous-manganous ions: a noticeable Mn(III) oxidation process. Water Res. 133, 227–235. https://doi.org/10.1016/j.watres.2018. 01.039.

Zhang, K., Sun, P., Faye, M.C.A.S., Zhang, Y., 2018b. Characterization of biochar derived from rice husks and its potential in chlorobenzene degradation. Carbon 130, 730–740. https://doi.org/10.1016/j.carbon.2018.01.036.

Zhang, K., Khan, A., Sun, P., Zhang, Y., Taraqqi-A-Kamal, A., Zhang, Y., 2019a. Simultaneous reduction of Cr(VI) and oxidization of organic pollutants by rice husk derived biochar and the interactive influences of coexisting Cr(VI). Sci. Total Environ. 135763. https://doi.org/10.1016/j.scitotenv.2019.135763.

Zhang, K., Sun, P., Zhang, Y., 2019b. Decontamination of Cr(VI) facilitated formation of persistent free radicals on rice husk derived biochar. Front. Environ. Sci. Eng. 13 (2). https://doi.org/10.1007/s11783-019-1106-7.

Zhong, D., Zhang, Y., Wang, L., Chen, J., Jiang, Y., Tsang, D.C.W., et al., 2018. Mechanistic insights into adsorption and reduction of hexavalent chromium from water using magnetic biochar composite: key roles of Fe_3O_4 and persistent free radicals. Environ. Pollut. 243, 1302–1309. https://doi.org/10.1016/j.envpol.2018.08.093.

Zhong, D., Jiang, Y., Zhao, Z., Wang, L., Chen, J., Ren, S., et al., 2019. pH dependence of arsenic oxidation by rice-husk-derived biochar: roles of redox-active moieties. Environ. Sci. Technol. 53, 9034–9044. https://doi.org/10.1021/acs.est.9b00756.